COMPARISON OF (NON-SLOTTED AND SLOTTED) SURFACE MOUNTED PM MOTORS AND AXIAL FLUX MOTORS FOR SUBMARINE SHIP DRIVES

Surong Huang Metin Aydin *Student Member* Thomas A. Lipo *Fellow, IEEE*

Department of Electrical and Computer Engineering
University of Wisconsin-Madison
1415 Engineering Drive
Madison, WI 53706-1691, U.S.A.

Abstract **-** The search for low noise motors for submersible ship operation has been pursued for many years. The main sources of the audible noise are the effects of slotting the stator which results in noise producing permeance harmonics and the placement of the windings resulting in noise producing MMF harmonics. These harmonics are the main reason for pulsating torque. To analyze pulsating torque, general instantaneous electromagnetic torque equation and torque ripple factor (TRF) were derived. Based on the torque and sizing analysis, optimum design can be achieved for minimum ripple torque and maximum torque density. PM pole arc ratio and magnet skew angle are chosen in order to both minimize the ripple torque and optimize the machine performance. The resultant plots are showed using 2D and 3D plots. Moreover, 2D and 3D Finite Element Analysis (FEA) of both axial flux and radial flux surface mounted motor structures (TORUS, KAMAN and RFSM) were investigated for pulsating torques, ripple torques and cogging torques. Results obtained from both sizing equations, TRF analysis and results obtained from 2D/3D FEA were completed and are illustrated in the paper.

I. INTRODUCTION

The search for a low noise motor for submersible ship operation has been sought for decades without a completely satisfactory solution. This difficulty has resulted from the emphasis which has been placed on the design of squirrel cage induction machines for such purposes. Unfortunately, induction machines, by their nature, have large number of inherent noise producing mechanisms due to the effects of slotting the stator and rotor. Consequently, these mechanisms cause noise producing permeance harmonics and necessitate placing windings in discrete slots resulting in noise producing MMF harmonics. The interaction between these two harmonic components produces additional force and torque producing harmonics and further complicates the issue. Finally, inverter-driven machines result in time harmonics impressed on the windings of the stator that can interact with the space harmonics to produce an additional measure of torque pulsations and audible noise.

One alternative to radial flux squirrel cage induction motors is a radial flux permanent magnet (PM) motor. Permanent magnet motors offer many advantageous features. They are usually more efficient because field excitation losses are eliminated. Rotor losses are reduced in PM machines compared to induction machines because they lack the rotor windings and field excitation in the rotor. Moreover, PM motors have small magnetic thickness which results in the fact that PM machines can be smaller than the other machines in terms of size. Therefore, the total mass of the machine goes down. However, these machines still contain noise and vibration sources. They also have the ability of developing magnetic stress in the machine airgap and various parts of the motor without use of stator current. One other alternative to radial flux machines are disc type axial flux PM machines [2-4]. These machines have been increasingly used in both naval and domestic applications as an alternative to conventional radial flux PM machines. Axial flux machines have numerous advantages over radial flux machines. These machines can be stacked axially allowing for a simple construction. The tape wound stator core can easily be manufactured. The airgap windings of the non-slotted axial flux machines require no slotted punching, and allows for surface shape of any kind. Improved torque/power density as well as reduced audible noise is unique features of these machines when compared with radial flux machines. There is no cogging torque due to

stator or rotor teeth with airgap type stator windings for the non-slotted axial flux machines and a relatively small cogging torque for the slotted axial flux machines. In addition, ripple torque is quite small compared to the radial flux PM machines. The coils can be designed for sinusoidal MMF and smooth torque with relatively quiet operation can be achieved. Moreover, the MMF harmonics can be further reduced by properly wrapping the airgap windings around the stator for the non-slotted topologies. Finally, cooling of the axial flux machines in non-slotted topologies is relatively easy since copper windings are exposed on the surface of the stator disc.

This paper develops and perfects the principles, analysis and calculation methods for the slotted and non-slotted permanent magnet motors for submersible shipboard applications. Specifically, these machines were evaluated from the perspective of noise, vibration, power density, efficiency, loss, and torque quality including torque ripple and cogging torque. Because of the application, care was taken to compare the results of various surface mounted permanent magnet motor topologies. The traditional radial flux surface mounted PM machine was chosen as a benchmark comparison in this study.

II. COMPARED MOTOR TYPES AND FEA MOTOR MODELS

Six different 200HP 1200rpm radial and axial flux type permanent magnet machines were analyzed in a recent study [1]. Two radial flux machines, namely non-slotted radial flux surface mounted PM machine (RFSM-NS) and slotted radial flux surface mounted PM machine (RFSM-S), were investigated. The rest of the machine types were axial flux surface mounted non-slotted and slotted one-stator-two-rotor (TORUS) and two-stator-one-rotor (KAMAN) type PM machines. In general, axial flux disc motors have N stators and N+1 rotors (N≥1) for external rotor & internal stator axial flux disc motor (TORUS) types and N+1 stators and N rotors (N≥2) for internal rotor & external stator axial flux disc motor (KAMAN) types. The machines analyzed in this paper are summarized and illustrated in Figure 1.

III. AN APPROACH TO MOTOR SIZING AND PERFORMANCE FOR COMPARISON OF MOTOR TYPES

In general, comparison of different machine types is a very formidable task. S. Huang et al [5] developed a general sizing and torque/power density equations and established a systematic method to compare the capabilities of machines with different topologies.

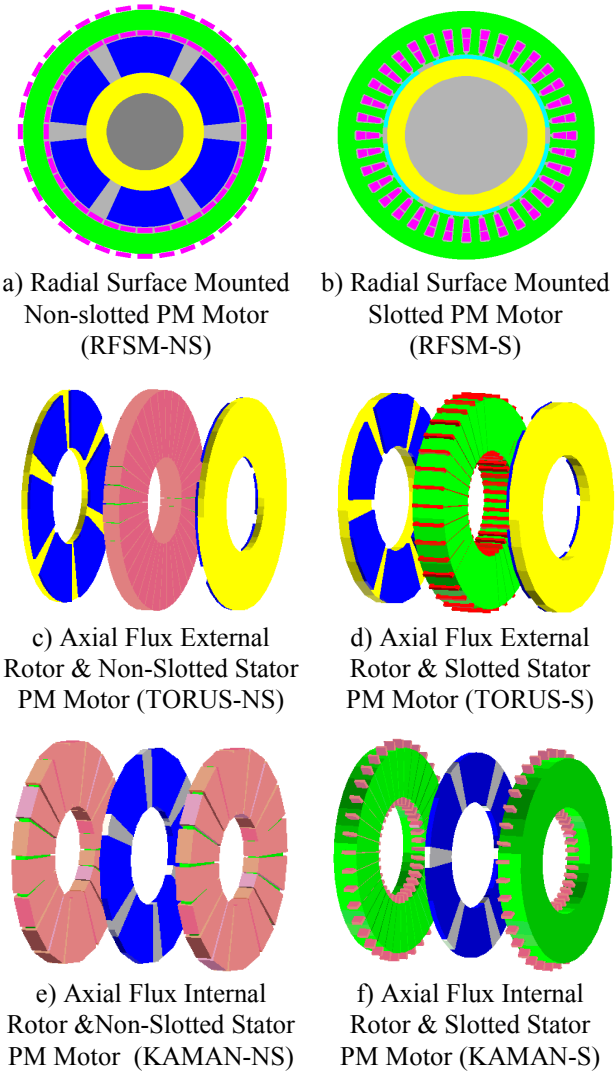

a) Radial Surface Mounted Non-slotted PM Motor (RFSM-NS)

b) Radial Surface Mounted Slotted PM Motor (RFSM-S)

c) Axial Flux External Rotor & Non-Slotted Stator PM Motor (TORUS-NS)

d) Axial Flux External Rotor & Slotted Stator PM Motor (TORUS-S)

e) Axial Flux Internal Rotor &Non-Slotted Stator PM Motor (KAMAN-NS)

f) Axial Flux Internal Rotor & Slotted Stator PM Motor (KAMAN-S)

Figure 1. Radial and Axial Flux PM Motor Models

In this section, first a concept was introduced in order to compare the torque density on the basis of total occupied volume instead of air-gap volume. Then special factors were presented to account for the effects of current and back-EMF waveforms. Finally the comparison methods were dedicated to the radial flux, the axial flux and the transverse flux machines respectively [5-7].

The general sizing equations have the following forms for both radial and axial flux machines:
For the radial flux machines [5]:

$$P_R = \frac{1}{1+K_\phi}\frac{m}{m_1}\frac{\pi}{2}K_e K_i K_p \eta B_g A \frac{f}{p}\lambda_o^2 D_o^2 L_e$$
$$= \frac{1}{1+K_\phi}\frac{m}{m_1}\frac{\pi}{2}K_e K_i K_p K_l \eta B_g A \frac{f}{p} D_g^3 \qquad (1)$$

and for the axial flux machines the sizing equations can be written in the following form [6]:

$$P_R = \frac{1}{1+K_\phi}\ \frac{m}{m_1}\ \frac{\pi}{2} K_e K_i K_p K_L\ \eta B_g A \frac{f}{p}\ (1-\lambda^2)\frac{1+\lambda}{2} D_o^{\,2} L_e \qquad (2)$$

where

P_R — rated output power of the machine,

$K_\phi = A_r / A_s$ — ratio of electrical loading on rotor and stator, in a machine without a rotor winding, $K_\phi = 0$,

m — number of phases of the machine,

m_1 — number of phases of each stator (if there is more than one stator, each stator has the same m_1),

K_e — EMF factor which incorporates the winding distribution factor K_w and the ratio between the area spanned by the (salient) poles and the total airgap area,

K_i — current waveform factor,

K_p — electrical power waveform factor,

η — machine efficiency,

B_g — flux density in the air gap,

A — total electrical loading,

f — converter frequency

p — machine pole pairs

L_e — effective stack length of the machine,

D_o, D_g, D_i — machine diameters at outer surface, air-gap surface and inner surface,

$K_l = L_e / D_g$ — aspect ratio coefficient for the radial flux machines,

$K_L = D_o / L_e$ — aspect ratio coefficient for the axial flux machines,

$\lambda_o = D_g / D_o$ — ratio of the diameter for radial flux machines,

$\lambda = D_i / D_o$ — ratio of the diameter for the axial flux machines.

Typical values for K_i and K_p are shown in Table 1.

Table 1 – Typical Prototype Waveforms

Model	*e(t)*	*i(t)*	K_i	K_p
Sinusoidal Waveform	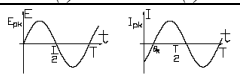		$\sqrt{2}$	.5cosφ
Sinusoidal Waveform	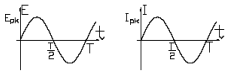		$\sqrt{2}$	0.5
Rectangular Waveform	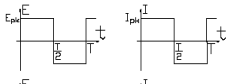		1	1
Trapezoidal Waveform	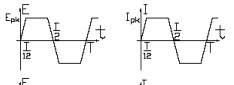		1.134	0.777
Triangular Waveform	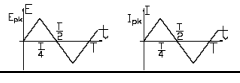		$\sqrt{3}$	0.333

The machine torque density and power density for the total volume can be defined as:

$$T_{den.} = \frac{T_R}{\frac{\pi}{4} D_{tot}^2 L_{tot}} = \frac{P_R}{\omega_m \frac{\pi}{4} D_{tot}^2 L_{tot}} \qquad (3)$$

$$P_{den.} = \frac{P_R}{\frac{\pi}{4} D_{tot}^2 L_{tot}} \qquad (4)$$

where T_R is the rated torque of the machine, D_{tot} is the total outer diameter of the machine including the stack outer diameter and the protrusion of the end winding from the iron stack in the radial direction, L_{tot} is the total length of the machine including the stack length and the protrusion of the end winding from the iron stack in the axial direction, ω_m is the rotor angular speed. In this case density ratio is defined as

$$\text{Density ratio} = \frac{T_{den.}}{T_{den.-RFSM}} = \frac{P_{den.}}{P_{den.-RFSM}} \qquad (5)$$

where $T_{den.\text{-}RFSM}$ and $P_{den.\text{-}RFSM}$ are the torque density and power density of RFSM machine respectively, as a benchmark for comparison of machine types.

Also, the utilization factor is expressed as

$$C_w = \frac{P_R(kW)\,.\,\eta}{W_{eight}(Kg)} \qquad (6)$$

where W_{eight} is the weight of the machines.

To consider the temperature rise, the heat dissipation factor is also given for both radial and axial machines:

$$Heat_{-diss} = \begin{cases} \dfrac{Copper\_loss + Iron\_loss}{\pi D_o L_{tot}} & \text{for RFSM} \\ \dfrac{Copper\_loss + Iron\_loss}{\pi(D_o + D_i)L_{stator} + 2(D_o^2 - D_i^2)\pi/4} & \text{for TORUS} \\ \dfrac{Copper\_loss + Iron\_loss}{2\pi(D_o + D_i)L_{stator} + 4(D_o^2 - D_i^2)\pi/4} & \text{for KAMAN} \end{cases} \qquad (7)$$

IV. GENERAL INSTANTENEOUS TORQUE EQUATION AND TORQUE RIPPLE FACTOR

Pulsation torque consists of two torque components: cogging torque and ripple torque. The cogging torque arises from the variation of the airgap permeance or reluctance of the stator teeth and slots above the magnets as the rotor rotates, while the ripple torque is mainly due to fluctuations of the field distribution and the armature MMF, which depends on the motor

structure and the armature current waveform. At high speeds, ripple torque is usually filtered out by the system inertia. However, at low speeds ripple torque produces noticeable effects that may not be tolerable in low noise and smooth torque applications. In the torque analysis, it was assumed that the motor is unsaturated, the airgap length is constant and the armature reaction is negligible. Also, the fundamental component of the armature current and the corresponding back EMF are assumed to be maintained in phase.

For the radial and axial flux motor, at instant t, the instantaneous torque produced by phase a is the interaction of the magnetic field $B(\theta_r, t)$ and the current $i_a(t)$ circulating in N conductors:

$$T_a(t) = i_a(t) 2pN \int_{-\pi/2mp}^{\pi/2mp} R_g L_e B(\theta_r, t) d\theta_r \qquad (8)$$

where $R_g = (D_o + D_i)/4$ is the mean airgap radius of axial flux machine or the airgap radius of radial flux machine, $L_e = (D_o - D_i)/2$ is the effective conductor length in radial direction of axial flux machine or the effective stack length of radial flux machine, p is the pole pair and m is number of machine phases.

The back-EMF induced in phase a at instant t is given by

$$e_a(t) = \omega_m 2pN \int_{-\pi/2mp}^{\pi/2mp} R_g L_e B(\theta_r, t) d\theta_r \qquad (9)$$

where ω_m is the rotor angular speed.

Substituting equation (9) into (8), the torque expression becomes

$$T_a(t) = \frac{e_a(t) \cdot i_a(t)}{\omega_m} \qquad (10)$$

For the Y-connected three-phase stator winding, the back-EMF in phase a can be written as

$$e_a = E_1 \sin \omega t + E_3 \sin 3\omega t + E_5 \sin 5\omega t + E_7 \sin 7\omega t + \ldots \qquad (11)$$

and the current in phase a can written as

$$i_a = I_1 \sin \omega t + I_5 \sin 5\omega t + I_7 \sin 7\omega t + I_{11} \sin 11\omega t + I_{13} \sin 13\omega t + \ldots \qquad (12)$$

where E_n is the n^{th} time harmonic peak value of EMF, which is produced by n^{th} space harmonic of the airgap magnetic flux density B_{gn}. I_n is the n^{th} time harmonic peak value of armature current which depends on the armature current waveform.

The product $e_a i_a$ consists of an average component and even-order harmonics for phase a

$$e_a i_a = P_0 + P_2 \cos 2\omega t + P_4 \cos 4\omega t + P_6 \cos 6\omega t + \ldots \qquad (13)$$

The total instantaneous torque is the sum of the torques produced by phase a, b, and c. That is,

$$T_{em}(t) = \frac{1}{\omega_m} [\, e_a(t) i_a(t) + e_b(t) i_b(t) + e_c(t) i_c(t) \,] \qquad (14)$$

Since the phase shifts between $e_a i_a$ and $e_b i_b$ and between $e_a i_a$ and $e_c i_c$ are $-2\pi/3$ and $2\pi/3$ respectively, the sum $(e_a i_a + e_b i_c + e_c i_c)$ contains an average component and harmonics of order of six. The other harmonics are eliminated. Therefore the instantaneous torque can be written as

$$T_{em}(t) = T_0 + \sum_{n=1}^{\infty} T_{6n} \cos n6\omega t \qquad (15)$$

where T_0 is the average torque and T_{6n} are the harmonic torques. The harmonic torques can be written as

$$T_0 = \frac{3}{2\omega_m} [E_1 I_1 + E_5 I_5 + E_7 I_7 + E_{11} I_{11} + E_{13} I_{13} + \ldots] \qquad (16)$$

$$T_6 = \frac{3}{2\omega_m} [I_1 (E_7 - E_5) + I_5 (E_{11} - E_1) + I_7 (E_1 + E_{13}) + I_{11} (E_5 + E_{17}) + \ldots] \qquad (17)$$

$$T_{12} = \frac{3}{2\omega_m} [I_1 (E_{13} - E_{11}) + I_5 (E_{17} - E_7) + I_7 (E_{19} - E_5) + I_{11} (E_{23} - E_1) + \ldots] \qquad (18)$$

$$T_{18} = \frac{3}{2\omega_m} [I_1 (E_{19} - E_{17}) + I_5 (E_{23} - E_{13}) + I_7 (E_{25} - E_{11}) + I_{11} (E_{29} - E_7) + \ldots] \qquad (19)$$

$$T_{24} = \frac{3}{2\omega_m} [I_1 (E_{25} - E_{23}) + I_5 (E_{29} - E_{19}) + I_7 (E_{31} - E_{17}) + I_{11} (E_{35} - E_{13}) + \ldots] \qquad (20)$$

From equations (15) through (20), one knows that in the ideal case if the back EMF's and the armature currents are sinusoidal, then the electromagnetic torque is

constant and no ripple torque exists. Since almost all-practical stator windings and PM field distribution have significant winding harmonics and flux density harmonics, induced back EMF's are non-sinusoidal and contain high-order harmonics. Consequently, ripple torque exists even with sinusoidal armature current source.

The torque-ripple factor (TRF) can be defined as the ratio of peak-to-peak ripple torque to average torque.

$$\text{TRF} = \frac{T_{pp}}{T_0} \tag{21}$$

where T_{pp} is peak-to-peak ripple torque which is given as

$$T_{pp} = 2\sqrt{T_6^2 + T_{12}^2 + T_{18}^2 + \ldots} \tag{22}$$

For the sinusoidal armature currents case, the torque-ripple factor expression becomes

$$\text{TRF} = 2\frac{\sqrt{(E_7 - E_5)^2 + (E_{13} - E_{11})^2 + (E_{19} - E_{17})^2 + (E_{25} - E_{23})^2 + \ldots}}{E_1}$$
$$= 2\frac{\sqrt{(K_{h7} - K_{h5})^2 + (K_{h13} - K_{h11})^2 + (K_{h19} - K_{h17})^2 + (K_{h25} - K_{h23})^2 + \ldots}}{K_{h1}} \tag{23}$$

where

$$\frac{E_n}{E_1} = \frac{K_{wn} \cdot K_{sn} \cdot K_{fn} \cdot K_{osn}}{K_{w1} \cdot K_{s1} \cdot K_{f1} \cdot K_{os1}} = \frac{K_{hn}}{K_{h1}},$$

and $K_{hn} = K_{wn}\, K_{sn}\, K_{fn}\, K_{osn}$ is n^{th} harmonic factor, $K_{w\,n}$ is the n^{th} harmonic winding factor, K_{fn} is the n^{th} harmonic form factor, K_{sn} is the n^{th} harmonic rotor skew factor and K_{osn} is the n^{th} harmonic open slot factor.

V. MINIMIZATION OF RIPPLE TORQUE FOR TORUS NON-SLOTTED MACHINE

For sinusoidal armature current case, because the ripple torque is proportional to the high-order harmonic component of EMF, it is possible to reduce the ripple torque to a minimum level by optimizing the PM shape and PM rotor skew angle. This principle was used in the optimization of the TORUS-NS machine. Analysis and calculation of torque ripple factor TRF and per unit average torque component vs. pole arc ratio $\alpha_i = w_{pm} / \tau_p$ and rotor PM pole skew angle θ_{skew} are shown from Figure 2 to 4. As can be seen from Figure 2, the TRF is minimum at a PM pole arc ratio of 0.81 as the electrical skew angle is 32.4 degrees. Figure 3 shows the average torque component as a function of PM pole arc ratio and electrical skew angle. It can be observed from the plot that average torque is quite high around the pole arc ratio of 0.81.

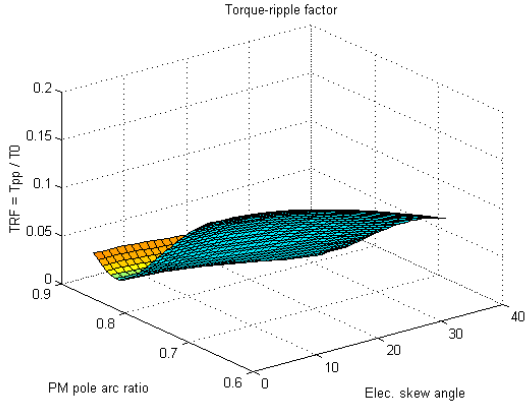

Figure 2. TRF vs. PM pole arc ratio α_i and rotor skew θ_{skew}

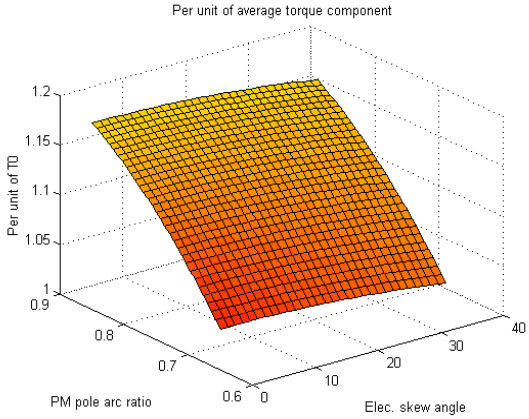

Figure 3. Per unit of average torque component vs. α_i and θ_{skew}

In addition, Figure 4 illustrates the 6th and 12th harmonic torque components vs. α_i and θ_{skew}. These plots show that the harmonic ripple torque curves are at a minimum near the pole arc ratio of 0.8 and electrical skew angle of 30 degrees.

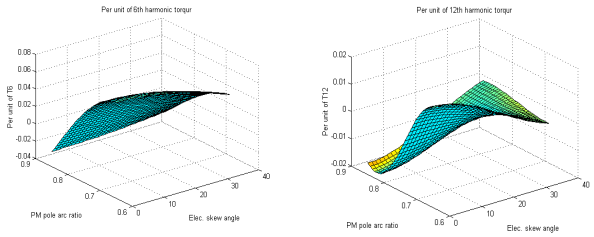

Figure 4. Per unit of 6th and 12th harmonic torque component vs. α_i and θ_{skew}

The same TRF plots are shown in 2D view in Figures 5 and 6 as well. Figure 5 shows the TRF as a function of the magnet pole arc ratio and the 6th and 12th harmonic torques in per unit. It can be observed from the plot that the TRF is minimum at a pole arc ratio of 0.81. Figure 6 illustrates the TRF, average torque and the amplitudes of different harmonic torques as a function of the electrical skew angle.

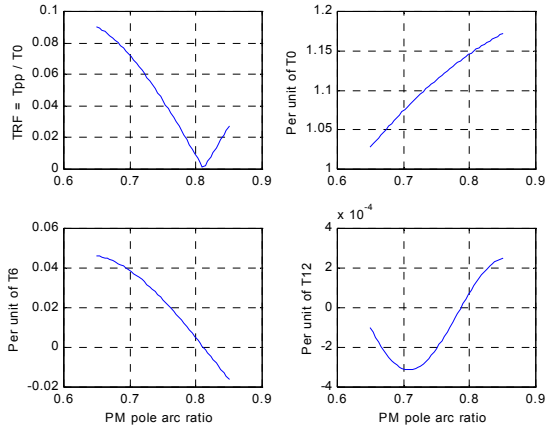

Figure 5. Per unit of harmonic torque vs. PM pole arc ratio

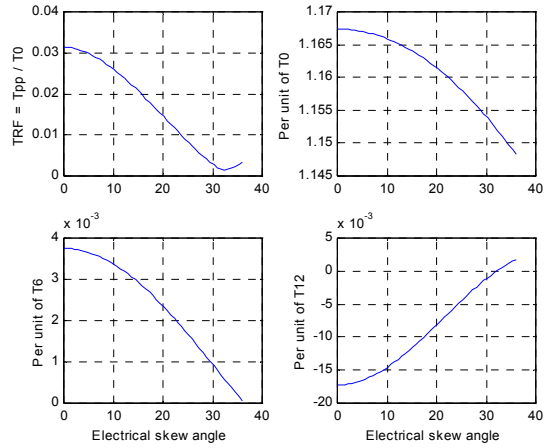

Figure 6. Per unit of harmonic torque vs. Electrical skew angle

Figure 7 shows the total torque, ripple torque and harmonic torques of the 200HP 1200rpm TORUS-NS machine for optimum pole arc ratio and skewed rotor magnet case. It can be examined from the plot that the ripple torque of the non-slotted TORUS machine is very low. The peak-to-peak 6th and 12th harmonic torques have also unnoticeably small values compared to the rated torque of the machine.

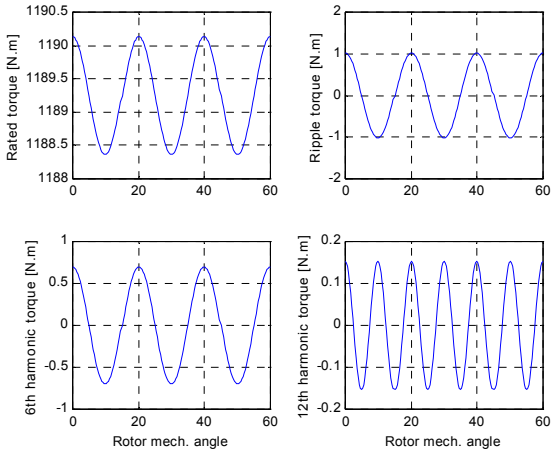

Figure 7. Torque vs. rotor position over one pole pair

Figure 8 shows the harmonic spectrum of the ripple torque in pu. As can be seen from the figure, the harmonic torques are multiples of 6 and the amplitudes are extremely low compared to the 1st harmonic.

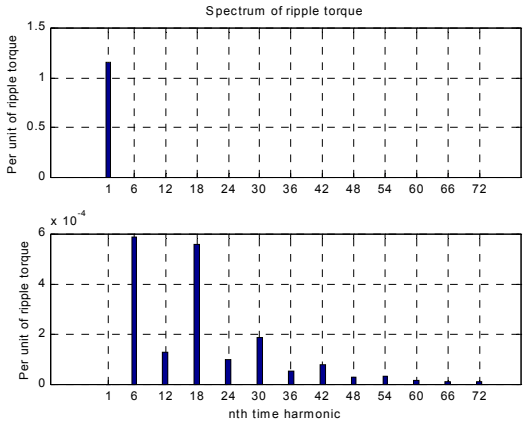

Figure 8. Spectrum of the ripple torque in [pu]

VI. TORQUE QUALITY AND COMPARISON USING FINITE ELEMENT ANALYSIS

A comparison of the topologies in terms of cogging torque and ripple torque was also realized for slotted and non-slotted machines using 2D and 3D Finite Element Analysis. The models were first operated at no load for different rotor positions and cogging torque variations were investigated. Pulsating torque values were then determined for the loaded case using the same approach. Since the ripple torque is defined as the difference between the pulsating torque and the cogging torque, the ripple torques of the machines can then be completed easily. Figure 9 shows the peak-to-peak cogging torque and ripple torque values for slotted topologies. It is interesting to note that the RFSM-S machine has the highest cogging torque even though slot

wedges were used in the model. From this analysis, it can be concluded that the cogging torque of the slotted axial flux machines are quite low compared to the radial flux machines if no slot wedge is used.

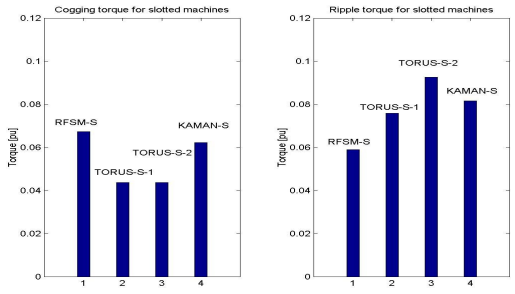

Figure 9. Comparison of cogging torque and ripple torque for slotted machines

Figure 10 shows the peak-to-peak values of cogging torque and ripple torque for non-slotted machines. It can be observed that radial flux surface mounted PM machine (RFSM-NS) has the highest ripple torque component compared to the other non-slotted topologies. Also, it can be deduced that the non-slotted machines have less ripple torque compared to slotted topologies.

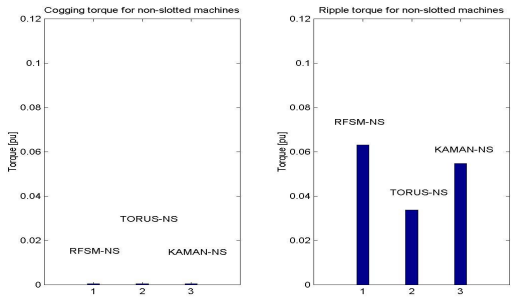

Figure 10. Comparison of cogging torque and ripple torque for non-slotted machines

VII. VIBRATION DISPLACEMENT DUE TO EXCITING FORCES

According as mechanical impedance method theory, the vibration displacement of the machine of the mode number and frequency concerned can be derived as

$$Y_{r/f_r} = \begin{cases} \dfrac{P_{eq-r/f_r}}{(k_{r-core}+k_{r-frame})-\omega_r^2\,(m_{r-core}+m_{r-frame})} & \text{for radial flux topologies} \\ \dfrac{P_{eq-r/f_r}}{k_{r-core-rotor}-\omega_r^2\,m_{r-core-rotor}} & \text{for TORUS topologies} \\ \dfrac{P_{eq-r/f_r}}{k_{r-core-stator}-\omega_r^2\,m_{r-core-stator}} & \text{for KAMAN topologies} \end{cases} \quad (24)$$

where P_{eq-r/f_r} is the equivalent exciting force in the airgap surface of the mode number and frequency concerned, $\omega_r = 2\pi f_r$ is the radian frequency of the exciting force waves, $k_{r-core-rotor}$ is the equivalent spring stiffness of the external rotor core including rotor PM for TORUS topology machines, $k_{r-core-stator}$ is the equivalent spring stiffness of the external stator core including stator windings and teeth for KAMAN topology machines.

The equivalent exciting force in the airgap surface for the mode number and frequency concerned is

$$P_{eq-r/f_r} = S_g\ P_{peak-r/f_r} \quad (25)$$

where P_{peak-r/f_r} is the amplitude of the exciting force waves for the mode number and frequency concerned. The airgap surface area is

$$S_g = \begin{cases} \pi D_g L_{eff} & \text{for radial flux topology} \\ \dfrac{\pi}{4}(D_0^2 - D_i^2) & \text{for axial flux topology} \end{cases} \quad (26)$$

According to Maxwell's equations, the magnitude of the exciting force is proportional to the square of the normal component of the air gap flux density.

$$p_{ef}(\theta,t) = \left\{ \frac{b^2(\theta,t)}{2\mu_0} \right. \quad (27)$$

where $p_{ef}(\theta,t)$ is the exciting force wave (force per unit area [N/m^2]), $b(\theta,t)$ is the air gap flux density waves, $\mu_0 = 4\pi\times10^{-7}$ [H/m] is the permeability of free space, θ is the space coordinate in radians. It should be noted that the exciting force is in the radial direction for radial flux machines and in the axial direction for axial flux machines in this equation. Also, the amplitude of the vibrating velocity of machine is given by

$$V_{pk-r} = \omega_r Y_{pk-r} \quad (28)$$

where Y_{pk-r} is the amplitude of the particle vibratory displacement and ω_r is the angular velocity of the sound wave.

VIII. RESULTANT SOUND POWER LEVEL

The surface vibration of machines due to the exciting force waves may be regarded as a series of rotating sinusoidal waves of displacement. Yang's (1975) equation of the sound power for the cylindrical sound wave model is [8].

$$W_{Cylin-r} = 2\rho C\pi^2 f_r^2 Y_{pk-r}^2 S_{Cylin} I_{re-r} \qquad (29)$$

where ρ is the density of the medium (for air $\rho = 1.186\, kg/m^3$), f_r is the frequency of the sound wave, C is the traveling speed of sound in the medium (for air, C =344 m/s), S_{Cylin} is the surface vibration area for the radial flux cylindrical machine which is perpendicular to the direction of travel of sound and I_{re-r} is the relative sound intensity coefficient.

The sound power for the plane sound wave model can be expressed as

$$W_{plane-r} = 2\rho C\pi^2 f_r^2 Y_{pk-r}^2 S_{plane} I_{re-r} \qquad (30)$$

where S_{Plane} is the surface vibration area for the axial flux disc machines and this area is perpendicular to the direction of the travel of sound. Finally the resultant sound power level is defined as

$$L_{Wt} = \sum_{i=1}^{n} L_{Wi} = 10\log\left[\sum_{i=1}^{n}\frac{W_i}{W_0}\right] = 10\log\left[\sum_{i=1}^{n} 10^{0.1L_{Wi}}\right] \text{ [dB]} \qquad (31)$$

where $L_{Wi} = 10\log\dfrac{W_i}{W_0}$ [dB], W_i is the sound power [w], $W_0 = 10^{-12}$ [w] is the reference value of the sound power.

IX. COMPARISON AND CONCLUSIONS

Sizing Analysis of 200 HP auxiliary motors was accomplished and the summary of the analysis is given in Figures 11a through 11e. The following conclusions can be obtained from the sizing analysis:

- TORUS slotted and non-slotted topologies have higher power or torque density ratio compared to other RFSM and KAMAN topologies.
- The efficiencies of all the topologies are quite high and very close to each other.
- KAMAN slotted and non-slotted topologies have the lowest weights among the others. Particularly, KAMAN-S topology has the lowest weight and highest utilization factor.
- Axial flux non-slotted topologies are always better than axial flux slotted topologies in terms of torque density, efficiency and heat dissipation.
- Internal rotor topology of axial flux machines can be easily used with cooling plate for conductor heat transfer.

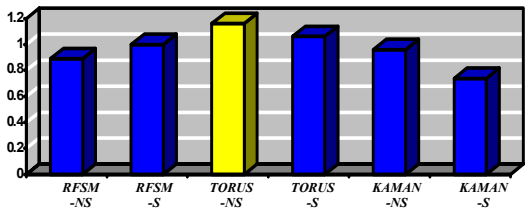

Figure 11a. Power/Torque Density Comparison [ratio]

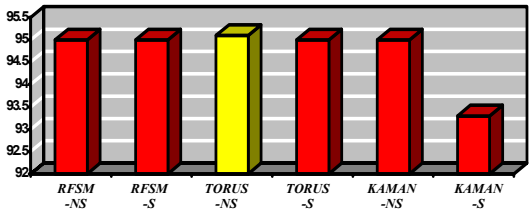

Figure 11b. Efficiency Comparison [%]

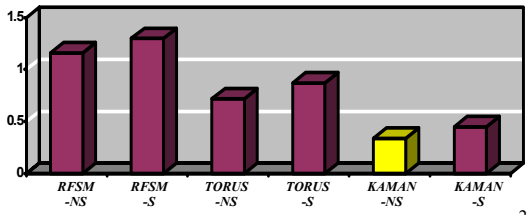

Figure 11c. Heat Dissipation Comparison [w/cm^2]

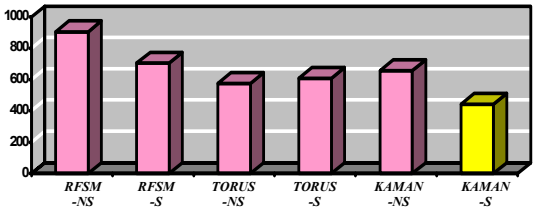

Figure 11d. Weight Comparison [lb]

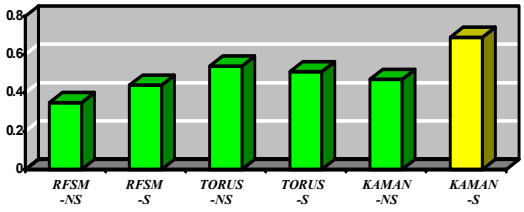

Figure 11e. Utilization Factor Comparison [kW/Kg]

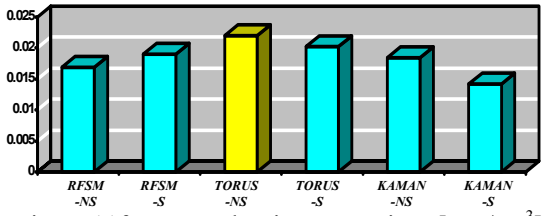

Figure 11f. Torque density comparison [Nm/cm^3]

Furthermore, finite element models were used to obtain the ripple torque and cogging torque characteristics of the machines. The results are shown from a different perspective in Figures 12 and 13 in pu without and with skewed rotor magnets. From this analysis, the following conclusions can be obtained:

- In general, non-slotted topologies have negligible cogging torque.
- The cogging torque is the highest for RFSM-S machine.
- Cogging torque can be reduced by skewing either rotor magnets or stator slots.
- In general, non-slotted machines have lower ripple torque than slotted machines for unskewed magnet case.
- TORUS-NS machine has the lowest ripple torque compared to the other topologies.

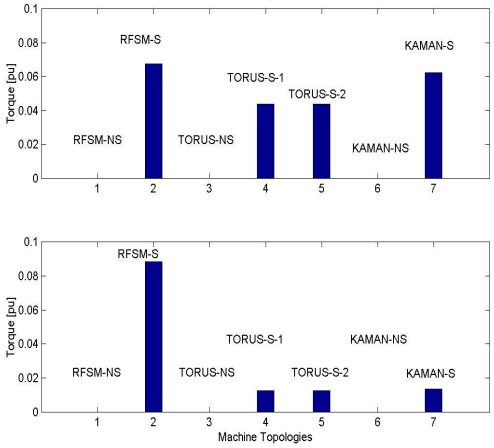

Figure 12.Cogging Torque Comparison without and with skewed rotor PMs [pu]

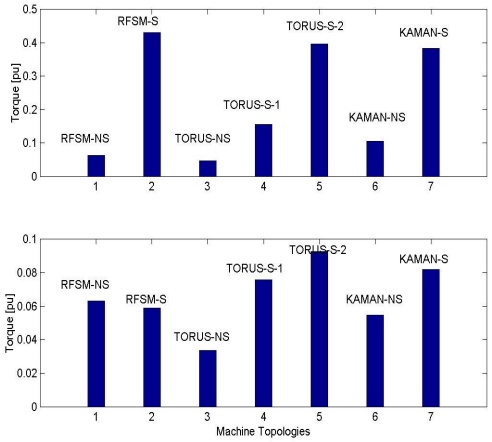

Figure 13. Ripple Torque Comparison without and with skewed rotor PMs [pu]

Finally, a detailed noise and vibration analysis was obtained. The resultant sound power levels, maximum vibration velocities and maximum vibration displacement of main vibration source values are shown in Figure 14a through Figure 14f. It should be noted that both high and low frequency ranges of vibration exist in any machine. The high frequency range of vibration is the main source of acoustics compared to low frequency range of vibration and causes the main acoustic noise that is in the range of the human ear. However, the low frequency range of vibration is the main vibration source compared to high frequency vibration. Skewing reduces the high frequency noise. As the thickness of the frame and core increased, the equivalent spring stiffness increases and results in reduced the low frequency vibration.

No Skewed Rotor PM – Full-load Case:

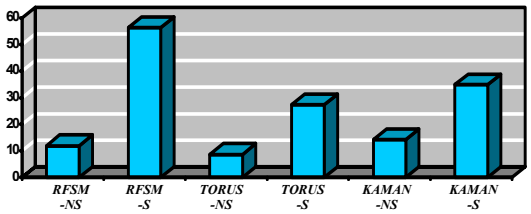

Figure 14a. Resultant Sound Power Level (L_{wr}) [dB]

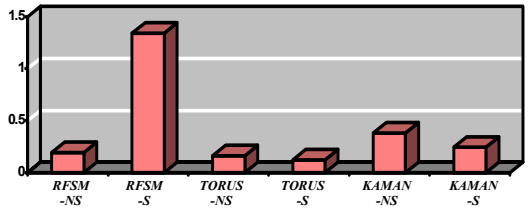

Figure 14b. Maximum Vibration Velocity of Main Vibration Source (*Vel_max*) [rms-mm/s]

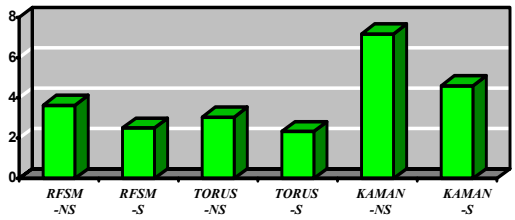

Figure 14c. Maximum Vibration Displacement of Main Vibration Source (*Y_max*) [peak-mm/s]

Skewed Rotor PM – Full-load Case:

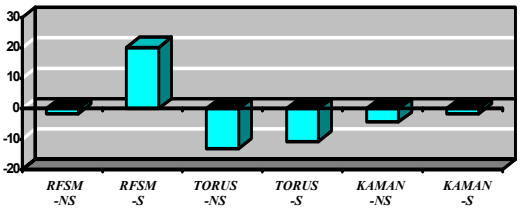

Figure 14d. Resultant Sound Power Level (L_{wr}) [dB]

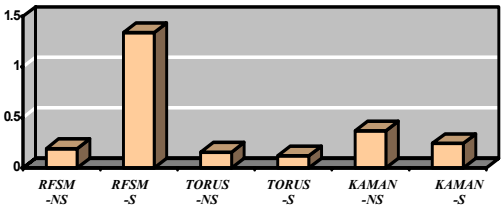

Figure 14e. Maximum Vibration Velocity of Main Vibration Source (*Vel_max*) [rms-mm/s]

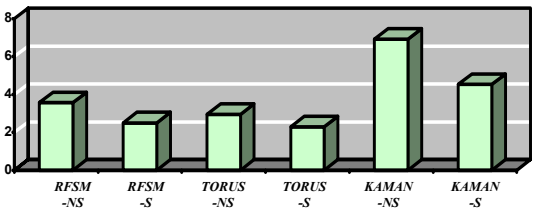

Figure 14f. Maximum Vibration Displacement of Main Vibration Source (*Y_max*) [peak-mm/s]

From this information and data gathered, following conclusions can be obtained:

- In general, non-slotted topologies have the lower sound power levels than slotted topologies. Especially, TORUS-NS topology has the lowest sound power level.
- Skewed rotor magnets reduce the noise level and high frequency vibration.
- TORUS-S machine has the highest spring stiffness and lowest vibration displacement.
- TORUS-NS machine has the highest torque/ power density, highest efficiency, lowest noise level and lower vibration displacement.
- The conventional radial flux slotted PM machine has the highest noise and vibration level.

X. ACKNOWLEDGEMENT

The authors wish to express their gratitude to the Office of Naval Research for their financial support of this research (Grant Number: N00014-98-1-0807).

REFERENCES

[1] T. A. Lipo, S Huang and M. Aydin, “Performance Assessment of Axial Flux Permanent Magnet Motors for Low Noise Applications”, Final Report to ONR, Oct 2000.

[2] P. Campbell, “Principles of a Permanent-Magnet Axial-Field DC Machine”, Proc. IEE, Vol. 121, No. 12, Dec. 1974, pp. 1489-1494.

[3] E. Spooner and B. J. Chalmers, “TORUS, A Toroidal-Stator, Permanent Magnet Machine for Small Scale Power Generation”, International Conference on Electrical Machines 1990, MIT, Cambridge, pp. 1053-1058.

[4] C. C. Jensen, F. Profumo and T. A. Lipo, “A Low Loss Permanent Magnet Brushless DC Motor Utilizing Tape Wound Amorphous Iron”, IEEE Transactions on Industry Applications, Vol. 28, No. 3, May/June 1992, pp. 646-651.

[5] S. Huang, J. Luo, F. Leonardi, and T. A. Lipo, “A General Approach to Sizing and Power Density Equations for Comparison of Electrical Machines,” IEEE Transactions on Industry Applications, IEEE Trans. IA-34, No.1, pp.92-97, 1998.

[6] S. Huang, J. Luo, F. Leonardi and T. A. Lipo, "A Comparison of Power Density for Axial Flux Machines Based on the General Purpose Sizing Equation", IEEE Trans. on Energy Conversion, Vol.14, No.2 June 1999, pp. 185-192.

[7] S. Huang, J. Luo and T. A. Lipo, ‘Analysis and evaluation of the transverse flux circumferential current machine’, Conference Record of the 1997 IEEE Industry Applications Society, 32nd IAS Annual Meeting, pp. 378-384.

[8] S.J. Yang, “Low-noise Electrical Motors”, Clarendon Press, Oxford, 1981.